



# Experimental investigation of heat transfer and pressure drop in metal-foam-filled circular and flattened tubes

Ehsan Rezaei<sup>1</sup> · Abbas Abbassi<sup>1</sup>

Received: 13 February 2020 / Accepted: 5 June 2020 / Published online: 29 June 2020  
© Akadémiai Kiadó, Budapest, Hungary 2020

## Abstract

Heat transfer and pressure drop of laminar flow inside circular and flattened tubes partially and fully filled with copper metal foam were experimentally investigated. The wall heated by a constant and uniform heat flux and water was used as the working fluid with Reynolds number ranging 500–2300. Six different configurations for tubes and porous media supposed and the Nusselt number and pressure drop data are reported and compared. The experimental results revealed that the porous media and flattening the tube have a significant effect on the thermal and hydrodynamic performances of the system due to the heat spreading through the copper matrix, better mixing of the fluid and extending the heat transfer area. Performance evaluation was carried out, and fully filled tubes were reported as having the best performance. The experimental data are also compared to well-known correlations from the literature, and new correlations are proposed to predict the Nusselt number and friction factor.

**Keywords** Convection · Experimental · Heat transfer · Pressure drop · Porous media · Flattened tube · Correlation

## List of symbols

$C_F$	Inertia parameter
$c_p$	Specific heat capacity ( $J\ kg^{-1}\ K^{-1}$ )
CT	Circular tube
$d_p$	Particle diameter (m)
$D$	Round tube diameter (m)
$D_h$	Hydraulic diameter (m)
EB	Energy balance
$f$	Friction factor
FT	Flat tube
$H$	Tube height (m)
$H_p$	Porous layer thickness (m)
$h$	Heat transfer coefficient ( $W\ m^{-2}\ K^{-1}$ )
$k$	Thermal conductivity ( $W\ m^{-1}\ K^{-1}$ )
$K$	Permeability ( $m^2$ )
$L$	Length of tube (m)
Nu	Nusselt number
$P$	Pressure ( $kg\ m^{-1}\ s^{-2}$ )
Pr	Prandtl number
$Q$	Total heat transfer rate ( $W\ m^{-2}\ K^{-1}$ )

$\dot{Q}_e$	Electrical heat ( $W\ m^{-2}\ K^{-1}$ )
$\dot{Q}_w$	Heat transfer rate to the water ( $W\ m^{-2}\ K^{-1}$ )
$q''$	Heat flux ( $W\ m^{-2}$ )
Re	Reynolds number
$T$	Temperature (K)
$t$	Pores thickness (m)
$V$	Velocity ( $m\ s^{-1}$ )
$W$	Width of the flat tube (m)
$Z$	Axial distance from the inlet (m)

## Greek symbols

$\alpha$	Thermal diffusivity ( $=k/\rho C_p$ ) ( $m^2\ s^{-1}$ )
$\epsilon$	Porosity
$\rho$	Density ( $kg\ m^{-3}$ )
$\rho_r$	Relative density
$\mu$	Dynamic viscosity ( $kg\ m^{-1}\ s^{-1}$ )
$\omega$	Pore density

## Subscripts

0	Round tube without porous
b	Bulk
i	Inlet
loc	local
mean	mean
p	Porous
s	Solid
t	Heat enhancement mechanism
w	Wall

✉ Ehsan Rezaei  
ehsanrezaei@aut.ac.ir

<sup>1</sup> Department of Mechanical Engineering, Amirkabir University of Technology (Tehran Polytechnic), 424 Hafez Ave, P.O. Box 15875-4413, Tehran, Iran

x	X direction
y	Y direction
z	Z direction

## Introduction

Today, with the improvement in industries and utilization of equipment with higher efficiency and greater thermal energy production, it is necessary that the heat transferability of cooling equipment to be more efficient. Therefore, traditional heat transfer methods will not meet future needs, and the necessity of new methods is feeling. The use of a special type of flat tubes, which has less thermal resistance than conventional circular pipes, is a different manner for increasing heat transfer in tubes. Adding a porous medium to the tubes is another way to increase the heat transfer, which, by reducing the hydrodynamic boundary layer, causes the increments in heat transfer. Combining the two methods of increasing the heat transfer and finding optimal flow conditions for a compromising between heat transfer and pressure drop is the main subject of the current study.

There are many researches focused on the forced convection in partially filled porous ducts and tube in different conditions [1–7]. The impact of many parameters like porous layer radius, Darcy number, Porosity, fluid–solid temperature difference (LTNE intensity), conductivity ratio and inertia factor on the pressure drop and heat transfer coefficient was investigated in these researches.

In an experimental research, Pavel and Mohamad [8] reported that using a porous insert with a lower porosity and greater thermal conductivity has a positive effect upon heat transfer and an undesirable influence on pressure drop. In an experimental study, Haung et al. [9] took into account the pressure drop and heat transfer in a wide range of flow regimes with different porosities. The results showed the 5.5-fold increment in heat transfer rate with the lowest porosity porous inserts in the laminar regime. Tu et al. [10], in an experimental research, investigated the influence of particle shape and particle size on the heat transfer rate. They realized that the spherical particle has a better effect on heat transfer enhancement than the dendritic particle, and there is an optimal value of particle size for the best PEC value. Also, the impact of particle shape and particle size on flow resistance is considered.

Open-cell metal foams, one of the useful types of porous structures, have attained more interest today. The major factors in heat transfer enhancement of metal foams are the high conductivity of solid structure, the potential capability of flow mixing and the large surface area per unit volume. Many researchers considered enhancing pressure drop and heat transfer by the use of metal foam in tubes. Lu et al. [11], by the use of the Darcy–Brinkman momentum model,

analytically investigated the heat transfer action of metal-foam-filled pipes for constant heat flux boundary conditions. The influences of relative porosity, density, pore density and thermal conductivity parameters on Nusselt number and pressure drop were examined. According to their results, up to 40 times increment in heat transfer was reported by the use of metal foam. Mancin et al. [12] experimentally provided the airflow and heat transfer through different copper and aluminum foams with various PPI, porosity and foam core heights at different airflow. They showed that the copper foams represented greater heat transfer action than the aluminum. In an experimental research, Bağcı and Dukhan [13] presented the pressure drop in two different aluminum metal foams in laminar and turbulent regimes based on the Reynolds number. They showed that in various post-Darcy flow trends, the values of the Forchheimer coefficient and permeability for metal foam are different. Also, the pore size and porosity have a negligible impact on the Darcy regime. Following the previous research, Dukhan et al. [14] considered all porous media flow regimes, Darcy, transitional and Forchheimer, and thermal entrance and thermal fully developed regions were detected. The results of analytical solution for LTNE condition and the experimental data had acceptable agreements and confirm that the LTNE assumption is ideal for simulating convection in metal foams.

Another method that helps heat transfer increment is applying flat tubes rather than common circular tubes. The flat tubes have a higher surface area to cross-sectional area ratio in comparison with the circular tubes utilized to the enhancement of the heat transfer and compactness of the system. In a numerical research, Vajjha et al. [15] considered nanofluid flow in an automobile radiators flat tube. Supposing convection heat transfer for the wall boundary condition, they suggested the association for the friction factor and local Nusselt number. In an experimental research, Razi et al. [16] studied the nanofluid heat transfer and pressure drop in several flat tubes and suggested correlations for pressure drop and Nusselt number. Safikhani and Abbassi [17] numerically assessed the influence of tube flattening on the fluid dynamic and heat transfer of nanofluid flow in different flat tubes with constant heat flux. In another work, Safikhani et al. [18], by the use of CFD, ANN and genetic algorithm, optimized the nanofluid flow in flat tubes. The design variables were the diameter of nanoparticles, internal height, heat flux, volumetric flow rate and nanoparticles volume fraction, and the final target was simultaneous increment in the coefficient of heat transfer and reduction in the pressure drop in flat tubes.

The present work, for the first time, examines the concurrent influences of a porous insert and flattening the tube on flow heat transfer and pressure drop experimentally. The numerical investigation of this study is presented in [19], and also the multi-objective optimization of design parameters

was studied [20]. Circular and flattened tubes are partially and fully filled with a porous medium with the wall connected to the persistent wall heat flux.

### Test setup details

Figures 1 and 2 represent the schematic of the test facilities, apparatus and tubes. The test section contains a horizontal copper tube of 1150 mm length and the wall thickness of

1.2 mm with an inside diameter of 10 mm for the round tube and an inside height of 6 mm for the flattened tube. The tubes were uniformly heated by a flexible electrical heating element wrapped around the tube while thermally insulated with 50-mm-thick glass wool (Fig. 3), and different heat flux was created by using a changeable AC power supply. To show the wall temperature profile, ten calibrated type T thermocouples (1 mm diameter and 100 mm length) were installed on the outer surface along the length of the tube and the distance between thermocouples was not uniform

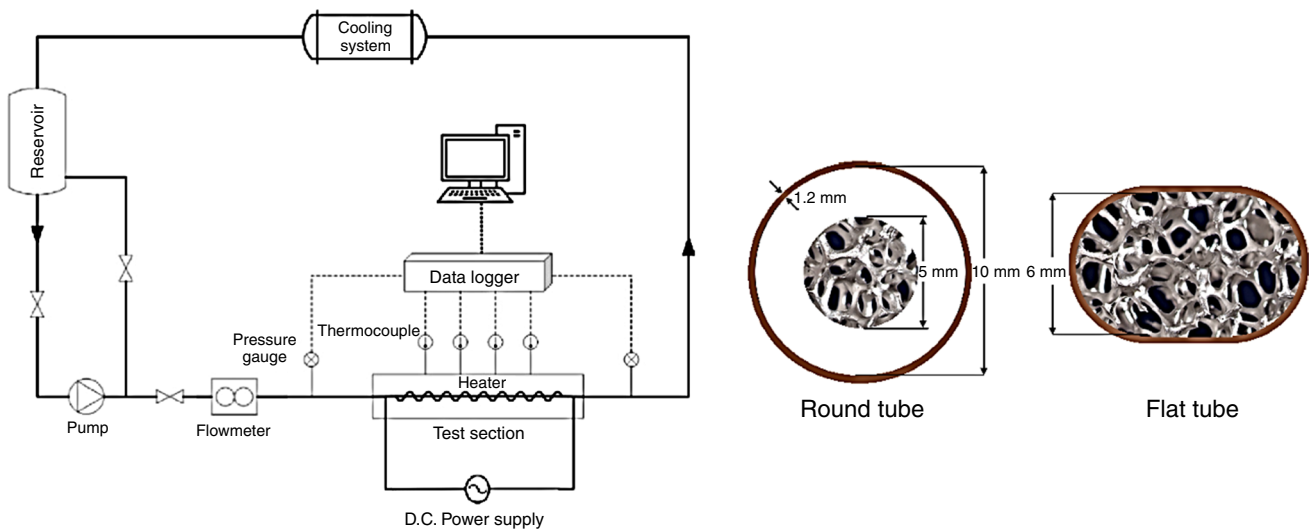


Fig. 1 Schematic of the test section

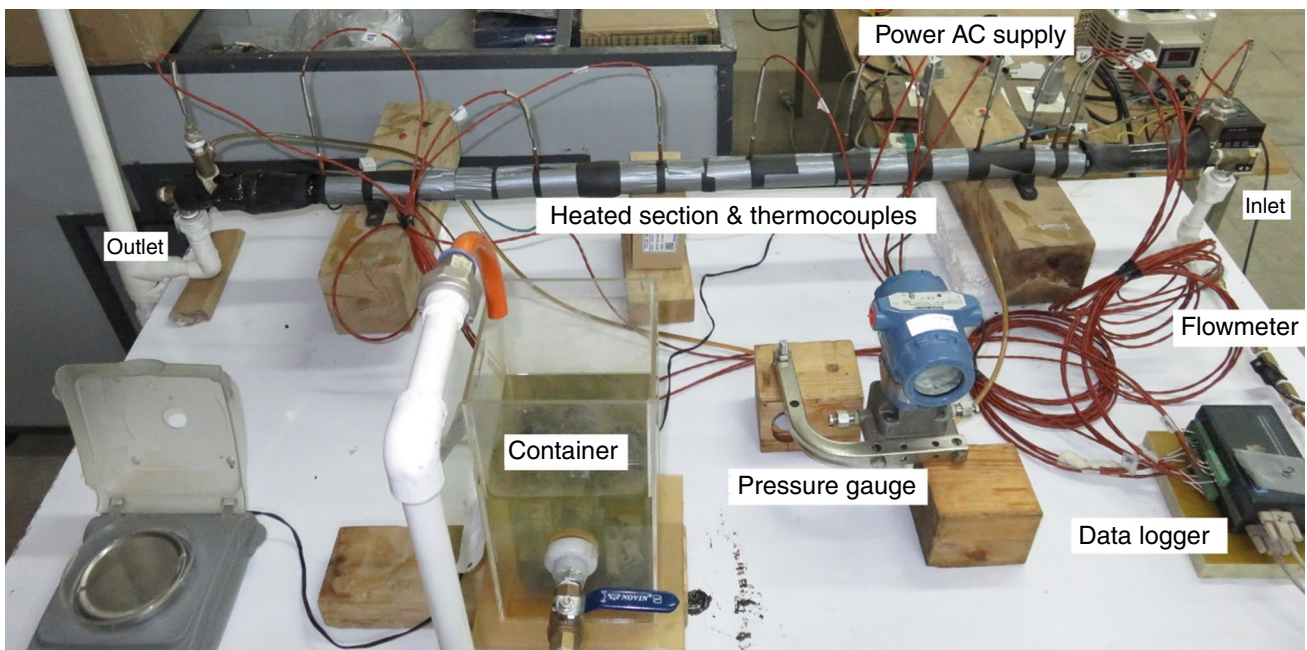


Fig. 2 Test rig and experimental apparatus



**Fig. 3** Copper tube, element heater and glass wool insulation

because of more variation at the entrance; therefore, the thermocouples were installed closer at this region. Two type T sensors measured the mean temperature of the inlet and outlet of the flow and all of the thermocouples connected to two Advantech 8-channel data loggers. A 3051-Rosemount pressure transmitter was also connected at the outlet and inlet of the test section. A reservoir made from plexi-glass is used as the main container of working fluid. About 5000 mL of distilled water flows uniformly inside a closed circuit with the aid of a gear pump with a maximum head and flow rate of 3.8 m and 9 m<sup>3</sup>h<sup>-1</sup>, respectively. A bypass line and a needle valve were used to adjust the flow rate to the tube in the range of 0.012–0.071 m<sup>3</sup>h<sup>-1</sup>. The LICO Vision 1000 flowmeter sensor was connected upstream of the test channel. A double-pipe counterflow heat exchanger with water forced on the cold side is used in the cooling unit. The heat exchanger was connected to the main water reservoir of the laboratory, and with control of the flow rate to the heat exchanger, the minimum temperature differences of input water of the main container were obtained. All of the experiments were performed at the inlet temperature of 25.5–27.5 °C. In order to more accurate flow rate measurement, with an Acculab milligram scale and CATIGA

stopwatch, for each input velocity, the flow rate was calculated and compared with other instruments. For each test, the flow rate was measured thrice before and after temperature and pressure readings. The test data were recorded after about 2.5 h to have steady-state condition. Table 1 lists the information and uncertainties of the main measuring instruments and dependent parameters.

## Porous media

The homogeneous open-cell copper metal foam is manufactured by deposition method (Fig. 4). Metal foam with constant porosity has the same length as the tube. In this experiment, two different cross sections of porous media, in the same form of the round and flattened tube with the radius ratio of  $\frac{D_p}{D}=0.5$  and 1 for round tube and the porous layer thickness ratio of  $\frac{H_p}{H}=1$  for flattened tube, were used. For the proper view of partially filled metal foam in the tube, Fig. 4 shows the porous media and the retaining wire passed through the center of porous. The parameters of the porous media testing sample are shown in Table 2. To evaluate the metal foam's porosity, Gibson and Ashby [21] procedure was used. According to Fig. 5, the tetrakaidecahedron structure can be used to describe the geometric specifications of metal foam cells. Based on the SEM image from the surface of metal foam (Fig. 5), by measuring the thickness ( $t$ ) and length ( $l$ ) of pores, the porosity of metal foam can be calculated by [21]:

$$\rho_r = 1 - \epsilon = 1.06 \frac{t^2}{l^2} \quad (1)$$

In this equation,  $\rho_r$  is the relative density. The permeability ( $K$ ) of metal foam testing sample can be related to pressure gradient and different velocity in the round tube with porous insert by the following equation [12]:

**Table 1** Specifications of instruments and apparatuses

Instruments	Company	Accuracy	Sensed parameter	Range	Specifications
Thermocouple	–	±0.5 °C or ±0.4%	$T_w, T_{in}, T_{out}$ (°C)	–250–350 °C	Type T
Data logger	Advantech thermocouple input, USB-4718-AE-USA	±0.1%	–	–100–400 °C	8-Channel USB
Flowmeter	LICO electronics turbine flowmeter—Switzerland	±3%	$Q$ (l/min)	0.1 – 2.5 l/min	Vision 1000
Differential pressure gauge	Rosemount—USA	±1.8 Pa or ±0.015%	$\Delta P$ (kPa)	–7.46 – 7.46 kPa	3051 °C
Differential pressure gauge	Rosemount—USA	±9.3 Pa or ±0.015%	$\Delta P$ (kPa)	0 – 62.27 kPa	3051
Scale	Acculab milligram scale—USA	±0.001 g or ±0.0003%	$m$ (kg)	0 – 300 g	VIC303
Flowmeter monitor	Autonics Pulse Meter—USA	±0.01%	$Q$ (l/min)	–	MP5W-F4
Chronometer	CATIGA stopwatch—China	±0.01 s or ±0.05%	$t$ (s)	0–20 s	CG-503



**Fig. 4** Copper metal foams, **a** circular tube with fully filled, **b** circular tube with partially filled, **c** flat tube with fully filled metal foam #2, **d** flat tube with fully filled metal foam #1, **e** metal foam and pores scale

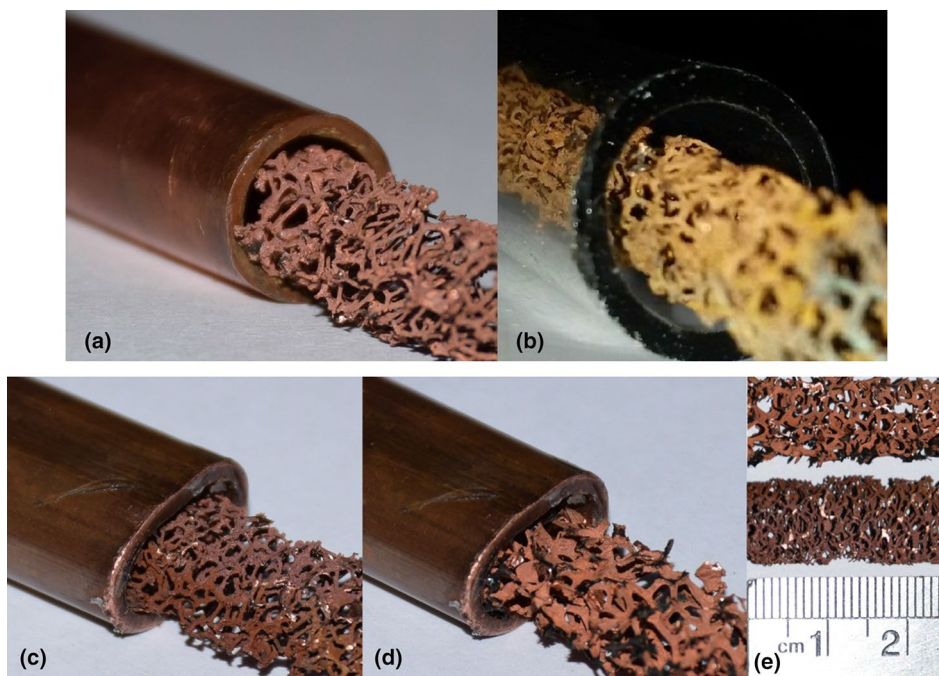


**Table 2** Metal foam samples details

Parameter	Metal foam #1	Metal foam #2
Porosity, $\epsilon$	0.828	0.976
Pore density, PPI	15	25
Permeability, $K/m^2$	$2.569 \times 10^{-8}$	$5.045 \times 10^{-8}$
Relative density, $\rho_R / \%$	17.155	2.385
Cell thickness, $t/mm$	0.561	0.225
Cell length, $l/mm$	1.354	1.458
Pore mean diameter, $d_p/mm$	4.862	2.301

$$\frac{dp}{dz} = \frac{\mu}{K} V + C_F \frac{\rho}{\sqrt{K}} V^2 \tag{2}$$

where  $C_F$  is the inertia factor. The permeability and friction factor were estimated by the least square error regression of measured data curve fitting and are presented in Table 2.

### Uncertainty analysis

The uncertainty analysis is performed to measure the errors of parameters such as length, temperature and heat flux. Uncertainties in this experimental research were estimated by the method suggested by Moffat [22] and are listed in Table 3.

The uncertainties of all parameters are computed as follows. If  $\{x_1, x_2, \dots, x_n\}$  are measured parameters and  $\{\delta x_1, \delta x_2, \dots, \delta x_n\}$  are their corresponding uncertainties, respectively, the uncertainty of  $f$  as a function of  $\{x_1, x_2, \dots, x_n\}$ ,  $f=f(x_1, x_2, \dots, x_n)$ , can be evaluated by:

$$\delta f_i = \pm \sqrt{\sum_{i=1}^n \left( \frac{\partial f}{\partial x_i} \delta x_i \right)^2} \tag{3}$$

The maximum uncertainty in the calculation of friction factor, heat transfer coefficient and Nusselt numbers is 4.4, 6.0 and 8.6%, respectively.

### Repeatability

Figure 6 represents the repeatability, one of the important specifications of any experiment which demonstrates the validity of the experimental work. This figure shows three records of wall temperature along the axial of the tube in four different conditions: round tube, flattened tube, round tube with porous insert and flattened tube with porous insert. The maximum and average deviations of the temperature in all the four conditions are 3.04% and 1.93%, respectively. According to the uncertainty of wall temperature, all the experiments and instruments are verified and repeatable.

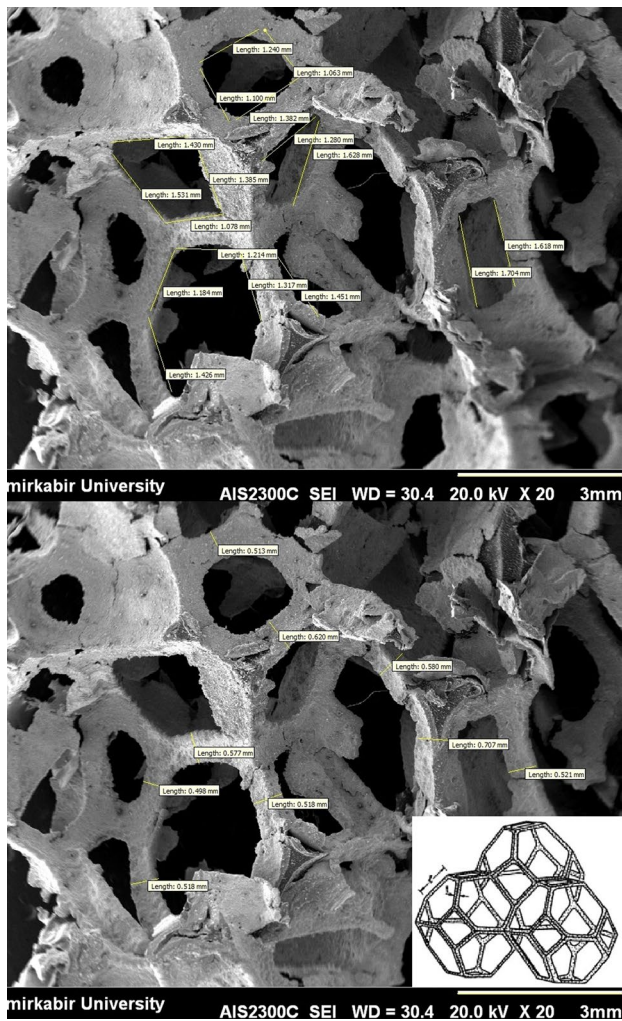


Fig. 5 SEM image of metal foam #1

## Data acquisition

The data processing is discussed in this section. The experimental conditions are demonstrated in Table 4. The water thermal specifications such as density, thermal conductivity, dynamic viscosity and specific thermal capacity were calculated based on bulk temperature with Popiel and Wojtkowiak [23] correlations. The average axial temperature of the water varied linearly because a constant heat flux is used for the tube wall. The bulk fluid temperature,  $T_b$ , is calculated as follows:

$$T_b = \left( \frac{T_0 - T_i}{2} \right) x + T_i. \quad (4)$$

The electrical heat supplied by a DC power is measured as follows:

$$\dot{Q}_e = VI. \quad (5)$$

Table 3 Uncertainty of all measured and derived parameters

Parameter	Maximum uncertainty (%)
Bulk temperature	± 6.0
Wall temperature	± 3.2
Voltage	± 0.2
Current	± 0.2
W, L, H	± 0.005
Thermal conductivity	± 6.2
Dynamic viscosity	± 1.0
Specific thermal capacity	± 0.06
Density	± 0.004
Pressure drop	± 0.2
Mass flow	± 1.3
Area	± 0.01
Cross section area	± 0.07
Hydraulic diameter	± 0.01
Reynolds number	± 4.4
Heat flux	± 0.3
Heat transfer coefficient	± 6.0
Nusselt number	± 8.6
Friction factor	± 4.4
Thermal performance index	± 6.0

And since the heat flux is constant,  $\dot{Q}_e$  remained constant. The heat transfer rate to the water is defined as follows:

$$\dot{Q}_w = mC_p(T_o - T_i). \quad (6)$$

$\dot{Q}_w$  is continuously compared to  $\dot{Q}_e$  to ensure the insulation of the test section. To be sure of the heat loss close to zero, the energy balance is determined as follows:

$$EB = \frac{\dot{Q}_e - \dot{Q}_w}{\dot{Q}_e} \times 100. \quad (7)$$

The energy balance of all the experiments was calculated by less than 7%. Therefore, in order to reduce the error associated with heat flux, the total heat transfer rate is defined as follows:

$$Q = \frac{\dot{Q}_e + \dot{Q}_w}{2} \quad (8)$$

The temperature differences across the tube wall,  $\Delta T$ , were calculated as follows:

$$\Delta T = \frac{\dot{Q}_w \ln\left(\frac{D_o}{D}\right)}{2\pi kL}. \quad (9)$$

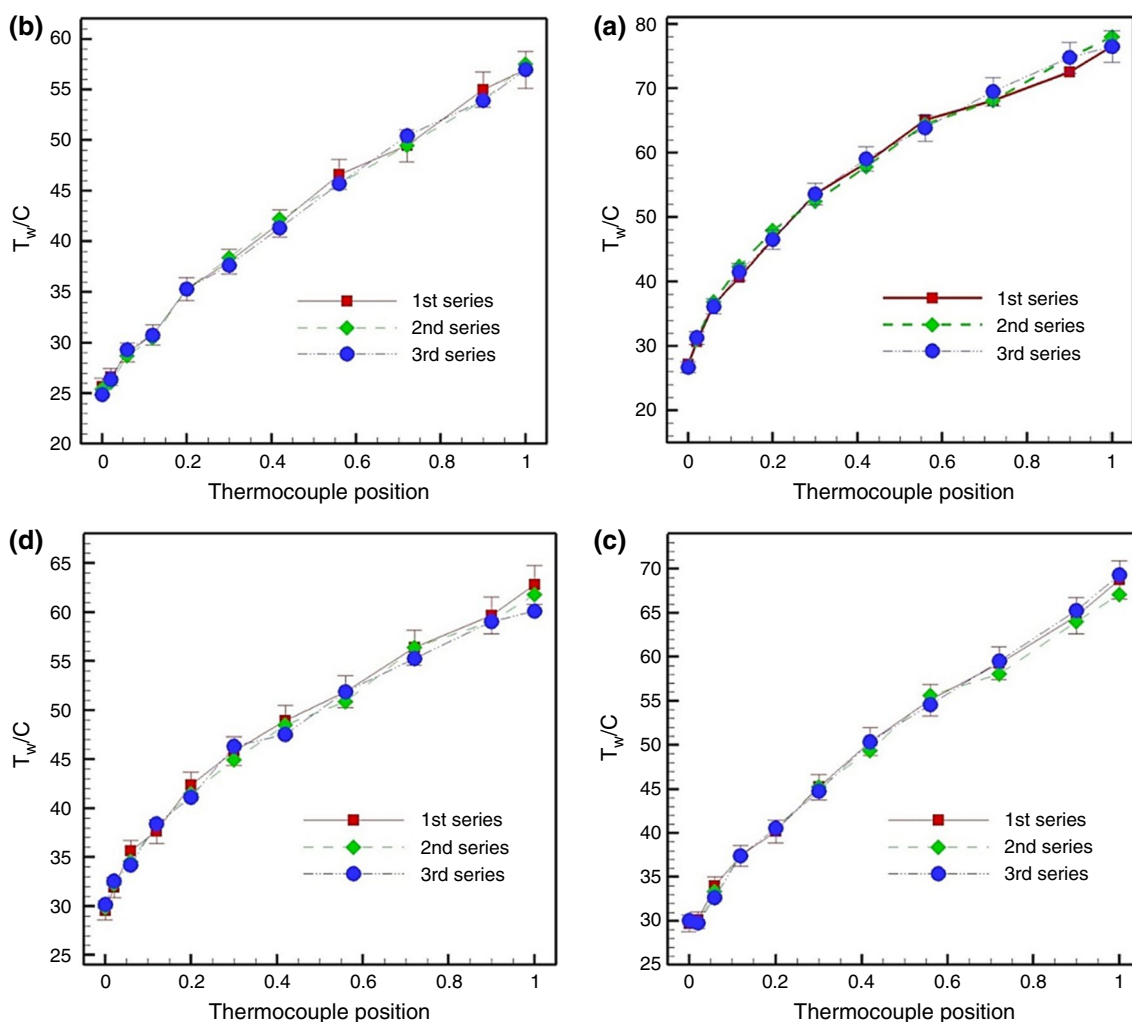


**Fig. 6** Repeatability for three measurements, **a** circular tube, **b** flat tube, **c** partially filled circular tube, **d** fully filled flat tube

This temperature difference at the maximum heat flux ( $2000 \text{ Wm}^{-2}$ ) was approximately  $0.004 \text{ }^\circ\text{C}$ . Since the temperature measurement accuracy was  $0.5 \text{ }^\circ\text{C}$ , the temperature difference across the tube wall could be neglected and it led to the assumption that the temperature on the inside and outside of the test section wall was equal.

The local heat transfer coefficient,  $h$ , and the mean heat transfer coefficients,  $h_{\text{mean}}$ , were determined from the following equations:

$$h = \frac{q''}{(T_w - T_b)} \tag{10}$$

$$h_{\text{mean}} = \frac{1}{L} \int_0^L h dz$$

The Nusselt numbers,  $\text{Nu}$ , were determined from the heat transfer coefficients:

$$\text{Nu} = \frac{hD_h}{k} \tag{11}$$

The average friction factors for tubes without porous media,  $f$ , across the different tube lengths can be calculated by Darcy–Weisbach:

$$f = \frac{2D\Delta P}{L\rho V^2} \tag{12}$$

where  $\Delta P$  is the measured pressure drop across the test section length  $L$ ,  $\rho$  is the density of the working fluid, and  $V$  is the flow velocity. The permeability friction factor for cases with porous media is defined as follows:

$$f_{\sqrt{K}} = \frac{\Delta P \sqrt{K}}{L\rho V^2} \tag{13}$$

**Table 4** Experimental conditions

Parameter	Value
Pipe material	Copper
Thermal conductivity/Wm <sup>-1</sup> K <sup>-1</sup>	401
Density/kg m <sup>-3</sup>	8960
Specific thermal capacity/Jkg <sup>-1</sup> K <sup>-1</sup>	385
Fluid type	Water
Inlet temperature/°C	25.5–27.5
Operating pressure/bar	1
Prandtl number	5.1–5.9
Reynolds number	500–2300

The Reynolds number, Re, and permeability Reynolds number,  $Re_{\sqrt{K}}$ , were calculated as follows:

$$Re = \frac{\rho VD}{\mu} \tag{14}$$

$$Re_{\sqrt{K}} = \frac{\rho V \sqrt{K}}{\mu}. \tag{15}$$

**Validation**

The reliability of the system for flow and heat transfer is evaluated by considering the related researches and comparing with experimental data for round and flattened tubes. For round smooth tube with a constant heat flux boundary condition and laminar trend, Shah and London [24] represent the convection heat transfer characteristics and friction factor of the fluid flow. Figure 7 represents a suitable match between the experimental results and Shah equation data at Re=891. The maximum and average relative errors are 2.54% and 1.96% for Nusselt number and 5.66% and 3.21% for friction factor. For flattened tube, numerical investigation of the present work [19] is considered

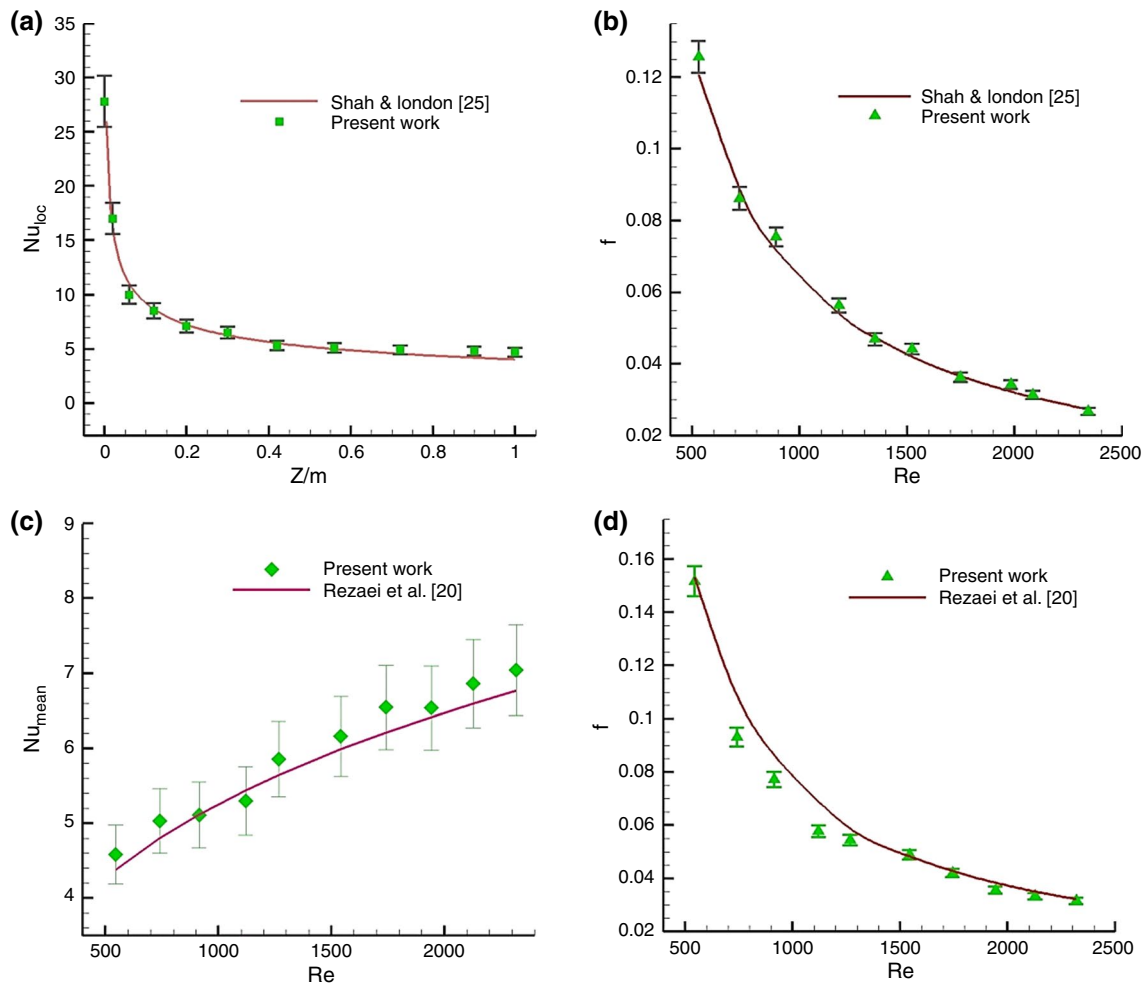


**Fig. 7** Validation of experimental data, **a** local Nusselt number for circular tube, **b** friction factor for circular tube, **c** mean Nusselt number for flattened tube, **d** friction factor for flattened tube



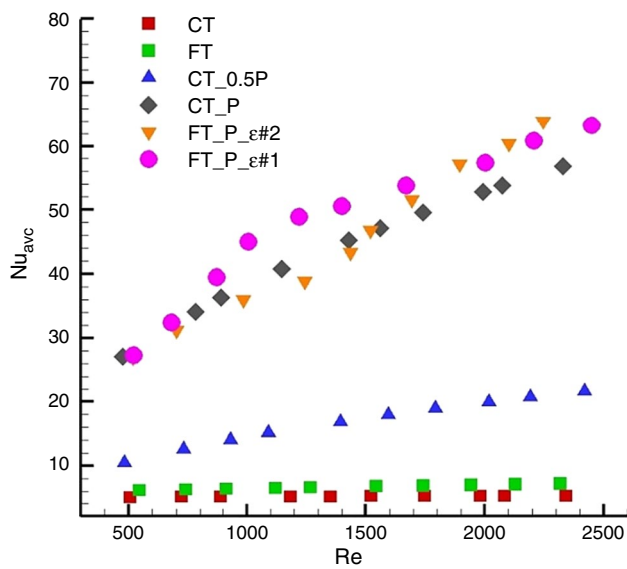


**Fig. 8** Variation of mean Nusselt number with the input flow rate for six configurations

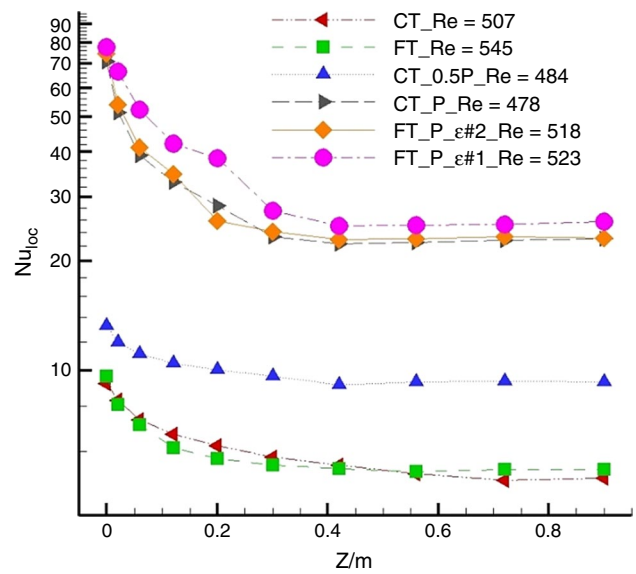
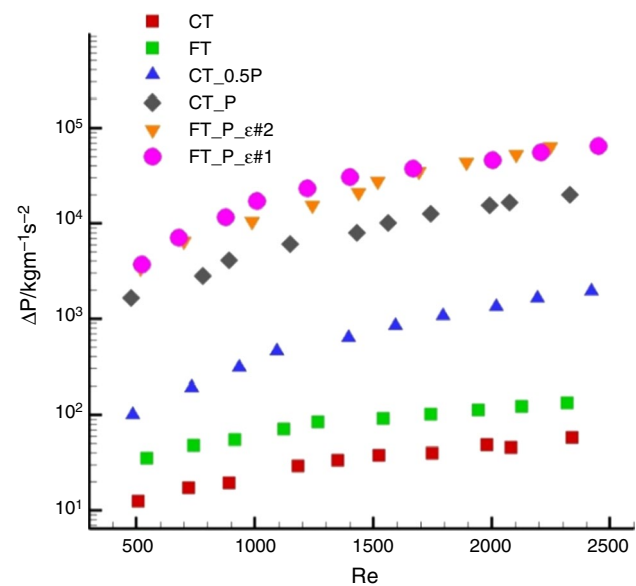


**Fig. 9** Variation of local Nusselt number with axial distance for six configurations

in comparison with experimental results. As shown in Fig. 7, the present experimental results are consistent well with the data reported by Rezaei et al. [19]. The maximum and average relative errors are 4.56% and 3.31% for Nusselt number and 13.41% and 7.58% for friction factor. The probable reasons for the excessive error of friction factor are different input boundary conditions in numerical simulations and experimental studies and their effect on hydrodynamic behavior of fluid flow in the pipe, probably diversity in flattening throughout the tube and various errors in the experiments.

### Results and discussion

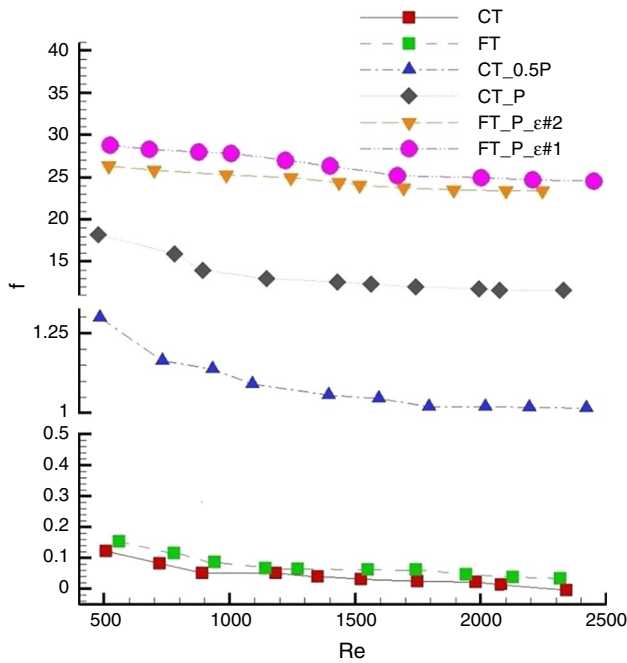
Experiments were done in ten volume flow rate 0.012–0.071 ( $\text{m}^3\text{h}^{-1}$ ) with the corresponding Reynolds number of 500–2300. As mentioned, six configurations of tubes and porous media were considered. CT: circular tube without porous, FT: flat tube with  $H=6$  mm and without porous, CT-0.5P: circular tube with partially filled porous media  $H_p=0.5$  and  $\epsilon=0.976$ , CT-P: circular tube with fully filled porous media  $H_p=1$  and  $\epsilon=0.976$ , FT-P#1 : flat tube with  $H=6$  mm and fully filled porous media  $H_p=1$  and  $\epsilon=0.828$  and FT-P#1: flat tube with  $H=6$  mm and fully filled porous media  $H_p=1$  and  $\epsilon=0.976$ .



**Fig. 10** Variation of pressure drop with the input flow rate for six configurations

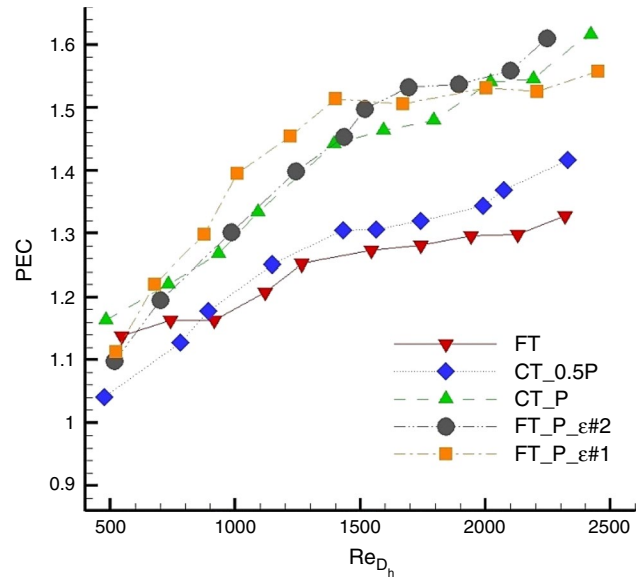
### Heat transfer

Figure 8 demonstrates the variation of mean Nusselt number with flow rates for all configurations. It is clear that the mean Nusselt number strongly relevant to flow rate based



**Fig. 11** Variation of friction factor with input flow rate for six configurations

on fluid bulk and wall temperatures changes due to the change in input flow rate. As shown in Fig. 8, flattening of the tube and adding porous layer by changing the temperature and velocity along the tube cross section dramatically increases the heat transfer. At high flow rate, the Nusselt number of FT, CT-0.5P, CT-P, FT-P#1 and FT-P#2 was calculated as 1.64, 4.11, 10.77, 14.44 and 14.27 times of CT, respectively. These results are consistent with those of Rezaei et al. [19]. It is obvious that the best thermal enhancement mechanism is the flattened tube fully filled with  $\epsilon = 0.828$  metal foam. This may be caused by the simultaneous effect of the surface area and the effective thermal conductivity according to the lower porosity. The local Nusselt number variation at Reynolds number close to 500 is shown in Fig. 9. The trend of local Nusselt number increment is similar to Fig. 8. As expected, the local Nusselt number is much more in entry regions than in fully developed regions because of boundary layer effects. Also, according to the figure, it is clear that the length of the developing region decreases with the flattening of the tube, adding the porous medium and simultaneously flattening and adding the porous medium. The explanation for this decrement is that by adding the porous layer and also flattening the tube, the fluid flows more rapidly close to the wall, and thus the thermal boundary layer's thickness decreases.



**Fig. 12** PEC variations with Re number for five cases

### Pressure loss

The pressure drop measurements for six cases are shown in Fig. 10. As predicted, the pressure drop grows by increasing the Reynolds number. Also, the friction factors based on Eq. (12) are shown in Fig. 11. The results show that the tube flattening increases the pressure drop due to changes in the pattern of flow and the speed distribution, which leads to the increment of velocity gradient on the wall. On the other

**Table 5** Available correlations for circular tubes fully filled with metal foam

Calmidi and Mahajan [27]	$Nu = 0.52 Re^{0.5} Pr^{0.37}$
Kim et al. [28]	$h = \frac{13.73 \rho_f c_{pf} V}{\eta_s} Re^{-0.489} Pr^{-0.666} Da^{0.451}$
Noh et al. [29]	$Nu = 23.1 Re^{0.4} Pr^{-0.106} \left(\frac{K}{L^2}\right)^{0.0935}$ $f = \frac{\mu D_h}{\rho V K} + \frac{0.05 D_h}{\sqrt{K}}$
Yang et al. [30]	$Nu = \frac{k_{stag} + \epsilon k_{dis}}{k_f} \times \left( \frac{8(\epsilon^* k_f + \epsilon k_{dis})}{k_{stag} + \epsilon k_{dis} - \frac{(1-\epsilon^*) k_s}{1 + \frac{16}{3} \left(\frac{2}{D_h}\right)^2}} \right)$
Wang and Go [31]	$f_k = 1/Re_k + 0.024$
Vafai and Tien [32]	$f_k = 1/Re_k + 0.057$
Dietrich (2012) [33]	$\frac{\Delta P}{\Delta L} = 110 \frac{\mu V}{\epsilon d_h^2} + 1.45 \frac{\rho V^2}{\epsilon^2 d_h}$

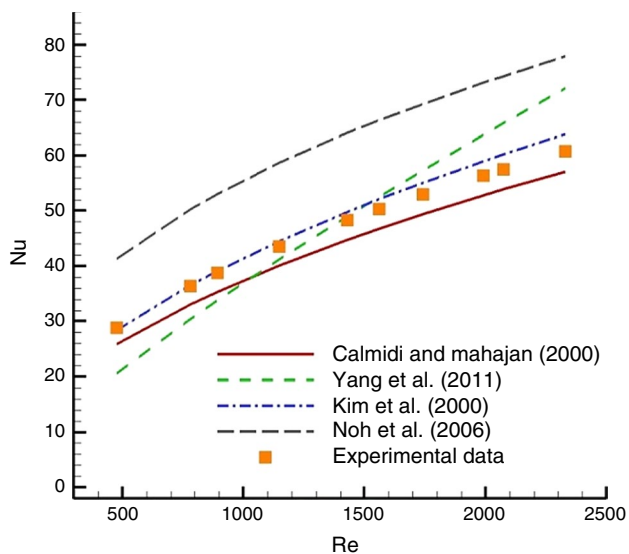


**Fig. 13** Comparison of experimental Nusselt number with other correlations

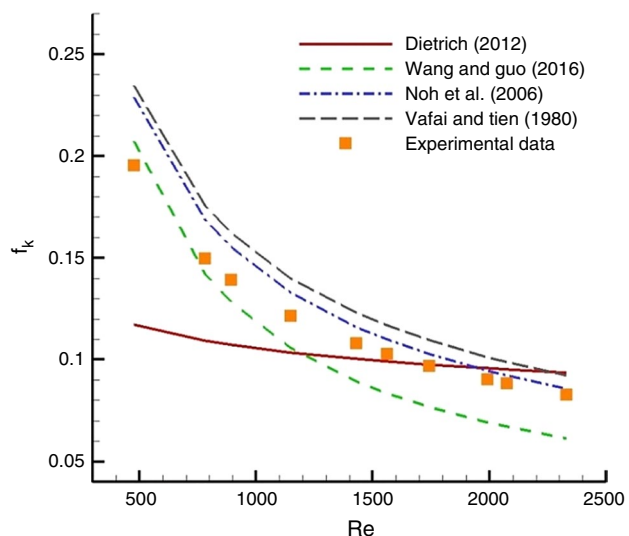


**Fig. 14** Comparison of experimental friction factor with other correlations

hand, the presence of the porous layer increases the water contact surface to the solid phase, which leads to more friction between the fluid and the contact surfaces. As shown in Fig. 10, the pressure drop due to the porous layer is greater than the flat tube effect. Also, the highest pressure drop was observed in the flat tube filled with metal foam with a

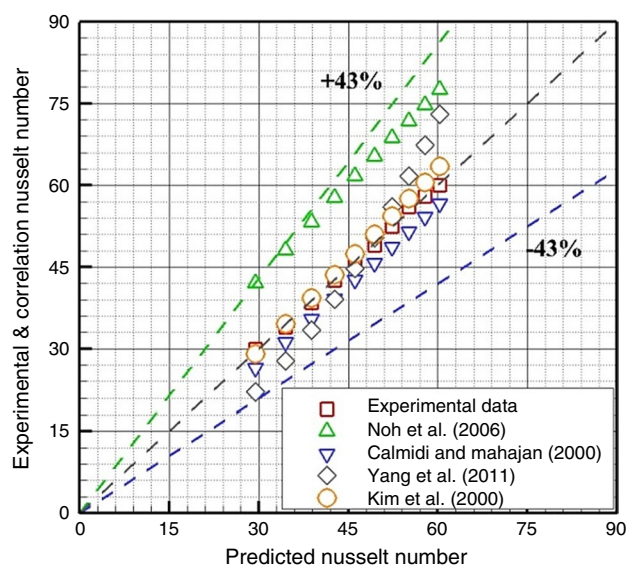


**Fig. 15** Comparison of Nusselt number of experimental and other correlations with the proposed correlation for circular metal-foam-filled tube

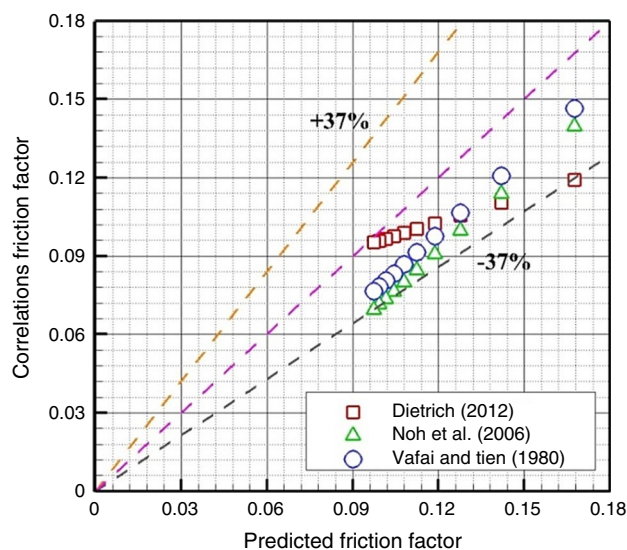


**Fig. 16** Comparison of friction factor of experimental and other correlations with the proposed correlation for circular metal-foam-filled tube

porosity of 0.882. At the highest flow rate, the pressure drops of FT, CT-0.5P, CT-P, FT-P#1 and FT-P#2 were calculated as 2.31, 33.61, 342.38, 1128.97 and 1097.03 times of CT, respectively. It is clear that similar to heat transfer,

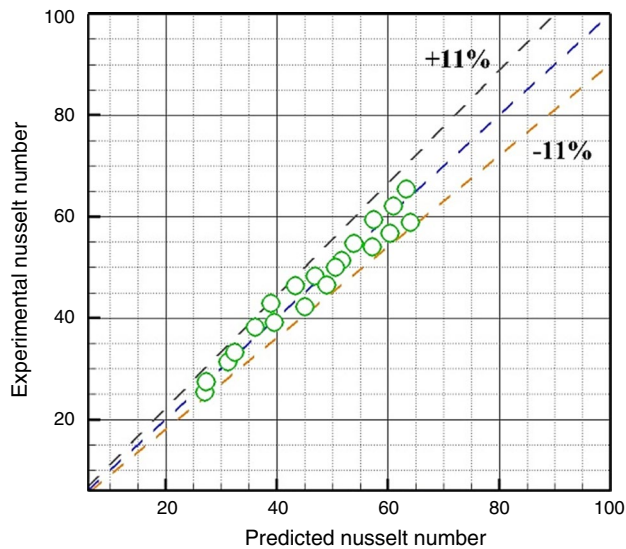


**Fig. 17** Comparison of experimental Nusselt number with the proposed correlation for the flattened metal-foam-filled tube

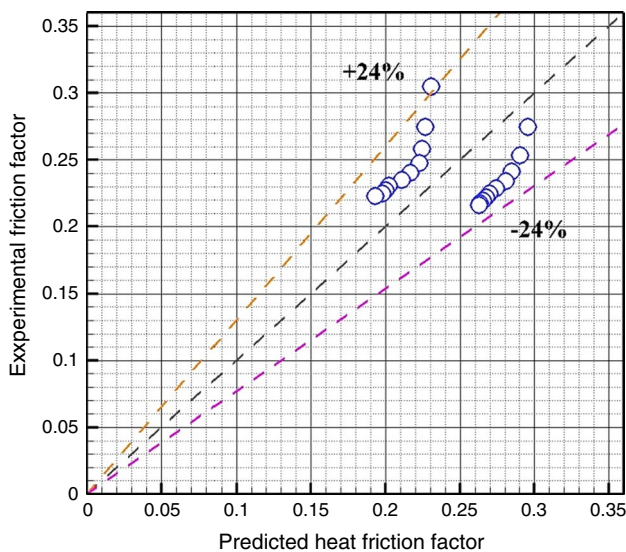


**Fig. 18** Comparison of experimental permeability friction factor with the proposed correlation for the flattened metal-foam-filled tube

the flattened tube fully filled with lower porosity has the maximum pressure drops.

In Fig. 11, the friction factor variations in six cases are shown in terms of the Reynolds number. As it is expected from the principles of fluid dynamics in a porous medium [25] and Fig. 11, the friction factor reduces steadily with increasing Reynolds number for circular and flattened tubes without a porous medium. For other cases, the reduction

in friction factor will be decreased or stopped from the Reynolds number range. This is due to the change in the flow regime inside the porous medium. Based on Bugci and Dukhan [13], completely turbulent flow initiates at around Reynolds number equal to 100 and friction factor will not be dependent on the Re.

### Performance index

As expected and shown in the previous section, flattening the tube and adding a porous layer increases the friction factor and the Nusselt number. The friction factor and the Nusselt number are two independent parameters which do not relate by any equation. In order to combine these two conflicted parameters, the thermal efficiency index is defined as follows [26]:

$$\eta = \left( \frac{Nu_t}{Nu_0} \right) / \left( \frac{f_t}{f_0} \right)^{1/3} \quad (16)$$

where  $t$  and  $0$  subscript refer to heat transfer mechanism and round tube without porous medium, respectively. The performance index for values larger than 1 represents the optimal state, and larger values show better performance.

The performance indexes for all cases based on the input flow rate variation are shown in Fig. 12. It is shown that the performance index increases by increasing inflow flow rate [28, 29] and the maximum value of  $\eta$  for the FT, CT-0.5P, CT-P, FT-P#1 and FT-P#2 is 1.32, 1.41, 1.62, 1.62 and 1.55, respectively. It is clear that up to Reynolds number of 900, the performance index for all cases does not have a trend and cannot be interpreted. In the Reynolds number range, 900–1500, FT-P#1 has the best performance index, and beyond the Reynolds number of 1500, FT-P#1 and CT-P have the best performance index.

### Correlations

In this section, for the round tube fully filled with porous media, the friction factors and heat transfer coefficient were compared with available correlations that are presented in Table 5. Based on the experimental data, the new correlations for circular and flat tube filled with porous media will be presented. Figure 13 compares the present experimental data with the results of Calmidi and Mahajan [30], Kim et al. [31], Noh et al. [32] and Yang et al. [33]. It is clear from Fig. 13 that the present experimental data have very good agreement with the other results. For example, between experimental results and those of Kim et al. [31], the mean error and maximum error were 3.32 and 5.43%, which indicates the high accuracy of experimental results.

The experimental permeability friction factor,  $f_k$ , was compared with available correlations, Wang and Guo [31],



Vafai and Tien [32] and Dietrich [33], and is presented in Fig. 14. It is clear that, similar to the heat transfer coefficient, experimental results have a good agreement with other results. For example, the experimental results and those of Noh et al. [29] have a mean error and maximum errors of 17.06 and 8.43%. The suitable match of the friction factor and Nusselt number with the predictive correlations validates the test section.

In order to predict the Nusselt number of water flow in a circular tube filled with a porous medium with a porosity of 0.976, based on the experimental data in terms of Reynolds number a new correlation is proposed:

$$Nu = 1.5927 Re^{0.4695} \quad (17)$$

The R-Square and main standard error are 0.999 and 1.127%, respectively. Figure 15 compares the Nusselt number of suggested model with the other correlations. Almost, all of the data fall within  $\pm 43\%$  of the forecasted values. Also, based on the experimental results, in terms of permeability Reynolds number a new correlation to predict the permeability friction factor of water flow in a circular tube filled with a porous medium with a porosity of 0.976 is proposed:

$$f_{\sqrt{k}} = \frac{1}{Re_{\sqrt{k}}} + 0.078. \quad (18)$$

The R-Square and main standard error are 0.997 and 2.241%, respectively. Figure 16 compares the friction factor of the proposed model with the other correlations. All of the data falls within  $\pm 37\%$  of the predicted values.

Since for the flattened tube with porous medium, no research has been done, there is not any correlation. According to the parameters of present experimental results, a relationship in terms of Reynolds number, Prandtl number and porosity can be reported as follows:

$$Nu = 0.394 Re^{0.413} Pr^{-1.019} \epsilon^{-0.426}. \quad (19)$$

The R-Square and main standard error are 0.968 and 5.391%, respectively. Figure 17 compares the experimental Nusselt number with that predicted by the correlation. Most of the investigational information is captured within a  $\pm 11\%$  error band.

The following correlation presented for the permeability friction factor of the laminar flow of water in the tube with flattening of  $H=6$  mm and fully filled metal foam:

$$f_{\sqrt{k}} = 1/Re_{\sqrt{k}} + 0.203. \quad (20)$$

The R-Square and main standard error are 0.928 and 6.637%, respectively. Figure 18 compares the permeability friction factor of the proposed model with the experimental data. All of data fall within  $\pm 24\%$  of the predicted values.

## Conclusions

Pressure drop and forced convection heat transfer of fluid flow inside a metal-foam-filled flattened tube have been experimentally evaluated in this paper for the first time. The effects of metal foam, flattening of the tube, Reynolds number and porosity of the metal foam on the heat transfer rate and pressure drop were investigated. The main findings of the paper can be concluded as follows.

- Flattening the tube and adding a porous layer remarkably increases the Nusselt number and the pressure drop.
- Both the Nusselt number and pressure drop indicate a strong dependence on the Reynolds number.
- The thermal entrance length of the fully developed area is distinguished by the local Nusselt number distribution. The thermal entrance length was determined to be shorter for flattened and fully filled metal foam tubes.
- The performance evaluation of the flat tube with fully filled metal foam is obtained. The results indicate that the PEC is remarkably influenced by Reynolds number and the mechanisms with the highest PEC changed in Reynolds number range. However, in all Reynolds number, fully filled metal foam mechanisms have the best PEC.
- Based on the results of the present experiments and the considered range of Reynolds numbers, the correlations between the average Nusselt number, Reynolds number and porosity for circular and flat tube were presented. Also, the correlations for friction factor based on the present experimental data were presented.

## References

1. Teamah MA, El-Maghlany WM, Khairat Dawood MM. Numerical simulation of laminar forced convection in horizontal pipe partially or completely filled with porous material. *Int J Therm Sci*. 2011;50:1512–22.
2. Dehghan M, Tajik Jamalabad M, Rashidi S. Analytical Nusselt number for forced convection inside a porous-filled tube with temperature-dependent thermal conductivity arising from high-temperature applications. *J Therm Analys Calorim*. 2020. <https://doi.org/10.1007/s10973-020-09667-y>.
3. Yang C, Liu W, Nakayama A. Forced convective heat transfer enhancement in a tube with its core partially filled with a porous medium. *Open Transp Phenom J*. 2009;1:6.
4. Yang C, Ando K, Nakayama A. A local thermal non-equilibrium analysis of fully developed forced convective flow in a tube filled with a porous medium. *Transp Porous Med*. 2011;89:237–49.
5. Mahmoudi Y, Karimi N. Numerical investigation of heat transfer enhancement in a pipe partially filled with a porous material under local thermal non-equilibrium condition. *Int J Heat Mass Transf*. 2014;68:161–73.
6. Mahdavi M, Saffar-Avval M, Tiari S, Mansoori Z. Entropy generation and heat transfer numerical analysis in pipes partially filled with porous medium. *Int J Heat Mass Transf*. 2014;79:496–506.

7. Shokouhmand H, Jam F, Salimpour MR. The effect of porous insert position on the enhanced heat transfer in partially filled channels. *Int Commun Heat Mass Transf.* 2011;38:1162–7.
8. Pavel BI, Mohamad AA. An experimental and numerical study on heat transfer enhancement for gas heat exchangers fitted with porous media. *Int J Heat Mass Transf.* 2004;47:4939–52.
9. Huang S, Wan Z, Wang Q, Tang Y, Yang X. Thermo-hydraulic characteristics of laminar flow in a circular tube with porous metal cylinder inserts. *Appl Therm Eng.* 2017;120:49–63.
10. Tu W, Wang Y, Tang Y. Thermal characteristic of a tube fitted with porous media inserts in the single phase flow. *Int J Therm Sci.* 2016;110:137–45.
11. Lu TJ, Stone HA, Ashby MF. Heat transfer in open-cell metal foams. *Acta Mater.* 1998;46:3619–35.
12. Mancin S, Zilio C, Diani A, Rossetto L. Air forced convection through metal foams experimental results and modeling. *Int J Heat Mass Transf.* 2013;62:112–23.
13. Bagci Ö, Dukhan N. Experimental hydrodynamics of high-porosity metal foam Effect of pore density. *Int J Heat Mass Transf.* 2016;103:879–85.
14. Dukhan N, Bagci Ö, Özdemir M. Thermal development in open-cell metal foam An experiment with constant wall heat flux. *Int J Heat Mass Transf.* 2015;85:852–9.
15. Vajjha RS, Das DK, Namburu PK. Numerical study of fluid dynamic and heat transfer performance of  $Al_2O_3$  and  $CuO$  nanofluids in the flat tubes of a radiator. *Int J Heat Fluid Flow.* 2010;31:613–21.
16. Razi PM, Akhavan-Behabadi A, Saeedinia M. Pressure drop and thermal characteristics of  $CuO$ -base oil nanofluid laminar flow in flattened tubes under constant heat flux. *Int Commun Heat Mass Transf.* 2011;38:964–71.
17. Safikhani H, Abbassi A. Effects of tube flattening on the fluid dynamic and heat transfer performance of nanofluid. *Adv Powd Technol.* 2014;25:1132–41.
18. Safikhani H, Abbassi A, Khalkhali A, Kalteh M. Multi-objective optimization of nanofluid flow in flat tubes using CFD, Artificial neural networks and genetic algorithms. *Adv Powd Technol.* 2014;25:1608–17.
19. Rezaei E, Abbassi A, Safikhani H. Numerical analysis of laminar heat transfer and fluid flow in a flat tube partially filled with a porous material. *J Porous Med.* 2018;21:1229–51.
20. Rezaei E, Abbassi A. (Under Publication) CFD Modeling and multi-objective optimization of flat tubes partially filled with porous layer using ANFIS, GMDH and NSGA II approaches. *AUT J Mech Eng.*
21. Gibson L, Ashby MF. Cellular solids structure and properties. Cambridge: Cambridge University Press; 1997.
22. Moffat RJ. Describing the uncertainties in experimental results. *Exp Therm Fluid Sci.* 1988;1:3–17.
23. Popiel CO, Wojtkowiak J. Simple formulas for thermophysical properties of liquid water for heat transfer calculations (from  $0^\circ C$  to  $150^\circ C$ ). *Heat Transf Eng.* 1998;19:87–101.
24. Shah RK, London AL. Laminar flow forced convection in ducts. New York: Academic Press; 1978.
25. Bear, J. Dynamics of fluids in porous media dovers. New York; 1972.
26. Webb RL. Performance evaluation criteria for use of enhanced heat transfer surfaces in heat exchanger design. *Int J Heat Mass Transf.* 1981;24:715–26.
27. Calmidi VV, Mahajan RL. Forced convection in high porosity metal foams. *J Heat Transf.* 2000;122:557–65.
28. Kim SY, Paek JW, Kang BH. Flow and Heat transfer correlations for porous fin in a plate-fin heat exchanger. *Heat Transf.* 2000;122:572–8.
29. Noh JS, Lee KB, Lee CG. Pressure loss and forced convective heat transfer in an annulus filled with aluminum foam. *Int Commun Heat Mass Transf.* 2006;33:434–44.
30. Yang C, Nakayama A, Liu W. Heat transfer performance assessment for forced convection in a tube partially filled with a porous medium. *Int J Therm Sci.* 2012;54:98–108.
31. Wang H, Guo L. Experimental investigation on pressure drop and heat transfer in metal foam filled tubes under convective boundary condition. *Chem Eng Sci.* 2016;155:438–48.
32. Vafai K, Tien CL. Boundary and inertia effects on convective mass transfer in porous media. *Int J Heat Mass Transf.* 1982;25:1183–90.
33. Dietrich B. Pressure drop correlation for ceramic and metal sponges. *Chem Eng Sci.* 2012;74:192–9.

**Publisher's Note** Springer Nature remains neutral with regard to jurisdictional claims in published maps and institutional affiliations.